EPJ Appl. Metamat. **6**, 3 (2019)

https://doi.org/10.1051/epjam/2018010

EPJ Applied Metamaterials

Available online at:
epjam.edp-open.org

Metamaterials Research and Development in Japan

RESEARCH ARTICLE OPEN ACCESS

Balanced gain for a square metaloop antenna

Hisamatsu Nakano*, Ittoku Yoshino, Tomoki Abe, and Junji Yamauchi

Science and Engineering, Hosei University, Koganei, Tokyo, Japan

Received: 29 August 2018 / Accepted: 3 December 2018

Abstract. A square loop antenna implemented using a metamaterial line, referred to as a metaloop, is discussed. The metaloop radiates a counter circularly polarized (CP) broadside beam when the loop circumference equals one guided wavelength. The frequency response of the gain shows two different maximum values: gain G_{Lmax} for a left-handed CP wave at frequency f_{GLmax} and gain G_{Rmax} for a right-handed CP wave at frequency f_{GRmax}, where G_{Lmax} is smaller than G_{Rmax}. In order to increase G_{Lmax}, while not affecting the original G_{Rmax} as much as possible (i.e. balance the gain), a parasitic natural conducting loop (paraloop), whose circumference is one free-space wavelength at f_{GLmax}, is placed at height H_{para} above the metaloop. It is found that the difference in the gains can be reduced by choosing an appropriate H_{para}. The radiation pattern at f_{GLmax} is narrowed by the paraloop, while the VSWR is not remarkably affected.

Keywords: Square metaloop antenna / circularly polarized radiation / gain balance

1 Introduction

A loop antenna radiates a linearly polarized (LP) wave [1]. When the circumference of the loop is one wavelength, the maximum LP radiation appears in the broadside direction. This broadside LP radiation can be changed to circularly polarized (CP) radiation by adding perturbation elements [2] to the loop, as shown in Figure 1. The rotational sense of the CP radiation, either a right-handed (RH) sense or a left-handed (LH) sense, is uniquely determined by the location of the perturbation elements relative to feed point F: the loop in Figure 1 radiates an RHCP wave. In other words, the loop antenna radiates a CP wave with a *single* rotational sense.

The single rotational sense also holds true for a grid loop array in [3]. Although perturbation elements are not added to the loops, a traveling current is generated along the arrayed loops and radiates a CP wave. The rotational sense is determined by the winding sense of the loops.

It is often required that an antenna has dual-band counter CP radiation to keep sufficient separation of signals, i.e., the LHCP and RHCP radiation in two different frequency bands, in order to avoid interfering with each other. When a pair of dual-band counter CP antennas is adopted as a transmitting antenna and a receiving antenna, it is desirable for these antennas to have the same gain. If the LHCP and RHCP gains are different, the receiving antenna captures LHCP and RHCP waves with different receiving power levels. Therefore, a post-process circuit connected to the receiving antenna needs additional amplification circuits to enhance the weak power. This complicates the post-process circuit designs. To avoid such an issue, the same gain (balanced gain) is desired.

Recent study has shown that a metamaterial (MTM) loop antenna, referred to as a metaloop, is an antenna that meets the requirement of dual-band counter CP radiation [4], where the loop is realized using the concept of a composite RH and LH transmission line [5–7], referred to as a metaline.

The maximum gain for the metaloop within the low frequency band (LoFB) in [4] is smaller than that within the high frequency band (HiFB). This is attributed to the antenna size relative to the free-space wavelength (electrical antenna size); the free-space wavelength within the LoFB is larger than that within the HiFB, and hence the electrical antenna size within the LoFB is smaller than that within the HiFB.

Thus, a question arises as to how the difference in the gains can be reduced. This paper presents a technique for reducing the band gain difference for a dual-band counter CP metaloop antenna, where a parasitic loop (paraloop) is placed above the metaloop. Note that the metaloop antenna in this paper is analyzed using a full wave analysis tool, HFSS [8], and experimental work is performed in an anechoic chamber.

So far, other authors have designed MTM-loaded and MTM-inspired loop antennas. For example, the MTM-loaded loop in reference [9] and MTM-inspired loop [10] are designed as an LP antenna. An antenna using complementary capacitively loaded loop in reference [11]

* e-mail: hymat@hosei.ac.jp

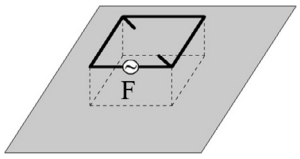

Fig. 1. Natural loop antennas radiating a circularly polarized wave with a single feed point F. The loop has perturbation elements [2].

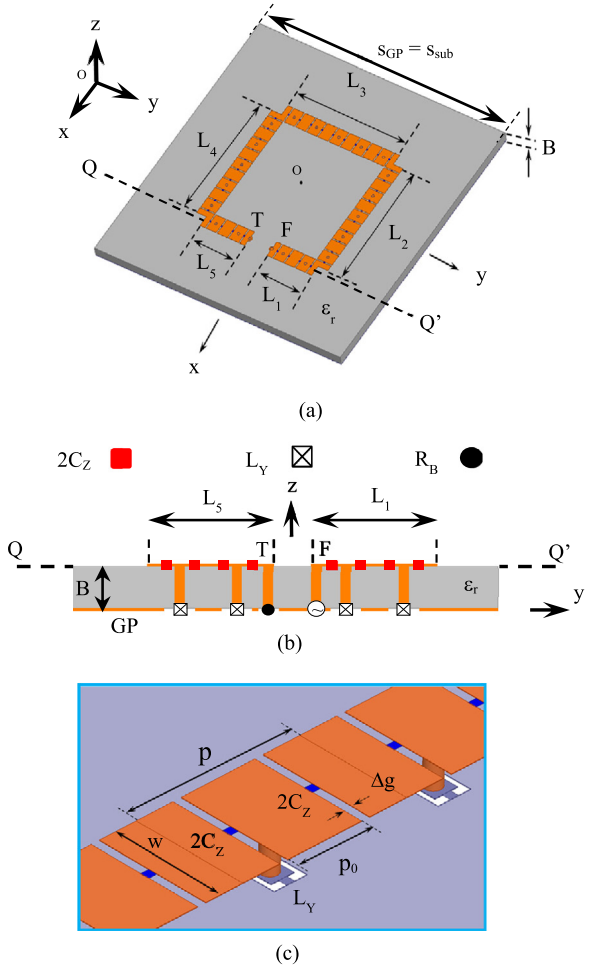

Fig. 2. Metaloop antenna. (a) Perspective view. (b) Side view. (c) Arm unit cell.

and loop antennas in [12–20] are also designed as an LP antenna. The design requirements for these antennas differ from ours, i.e., dual-band counter CP radiation with balanced gain, while meeting two additional requirements: (1) broadside radiation and (2) simple feed system without balun circuits. To our best knowledge, there have not been such MTM-related loop antennas.

2 Metaloop structure

The metaloop antenna to be considered here is shown in Figure 2. The antenna arm is printed on a square dielectric substrate of side length S_{sub}, relative permittivity ε_r and thickness B. The substrate is backed by a square ground plane (GP) of side length S_{GP} ($=S_{sub}$). The antenna arm, symmetric with respect to the x–z plane, is composed of five straight metalines, whose lengths are $L_1 = L_5$ and $L_2 = L_3 = L_4$. Each metaline is made of numerous conducting subwavelength segments of width w and length p_0, where the gap between neighboring segments is denoted as Δg. Repeating arm sections, each having length $2(\Delta g + p_0) \equiv p$, are designated as the arm unit cells. The central segment of the cell is short-circuited to the GP through a chip inductor, L_Y. Neighboring segments are connected through a chip capacitor, $2C_Z$. Point F is the feed point and point T is the terminal point connected to the GP through a resistive load, R_B, to suppress reflected currents from point T to point F.

Table 1. Parameters.

Symbol	Value	Symbol	Value
w	6.6 mm	p	10 mm
ε_r	2.6	p_0	4.5 mm
B	3.2 mm	Δg	0.5 mm
$L_1 = L_5$	20 mm	L_Y	1.8 nH
$L_2 = L_3 = L_4$	50 mm	$2C_Z$	1.2 pF
$S_{sub} = S_{GP}$	110 mm	R_B	60 Ω

Note that L_Y and $2C_Z$ are determined as follows. First, using HFSS [8], we obtain the frequency response of the scattering parameters (S-parameters) for the unit cell including L_Y and $2C_Z$. Second, based on the obtained S-parameters, we draw the dispersion curve (phase constant $\beta = \pm 2\pi/\lambda_g$ vs. frequency f [4], where λ_g is the guided wavelength). These two steps are repeated until the dispersion curve is balanced (smoothly connected at a preselected transition frequency f_T), changing L_Y and $2C_Z$. The values for L_Y and $2C_Z$ when the dispersion curve is balanced are what we need.

The parameters used for the following discussion are summarized in Table 1; these parameters create a preselected transition frequency of $f_T = 3$ GHz, i.e., phase constant β is negative at frequencies below f_T and positive at frequencies above f_T. Figure 3 shows the loop peripheral length $L_1 + L_2 + L_3 + L_4 + L_5$ normalized to the guided wave length, λ_g, as a function of frequency f. Note that the frequency-dependent guided wavelength λ_g used in Figure 3 is derived from the dispersion curve explained in the previous paragraph.

Frequencies f_L and f_U in Figure 3 are the lower- and upper-edge frequencies for a fast wave region. The radiation occurs between f_L and f_U. A traveling wave current flows along the loop from point F to point T, with guided wavelength λ_g, which varies with frequency f. The propagation phase constant is $\beta = -2\pi/\lambda_g < 0$ at $f < f_T$, $\beta = 0$ at $f = f_T$, and $\beta = 2\pi/\lambda_g > 0$ at $f > f_T$. In order to obtain a broadside beam at two different frequencies where the loop length is $1\lambda_g$, the in-phase condition ($\beta = 0$) is not used.

3 Frequency response of the gain

By resistive load R_B, a traveling wave current flows along the loop from point F to point T, with frequency-dependent

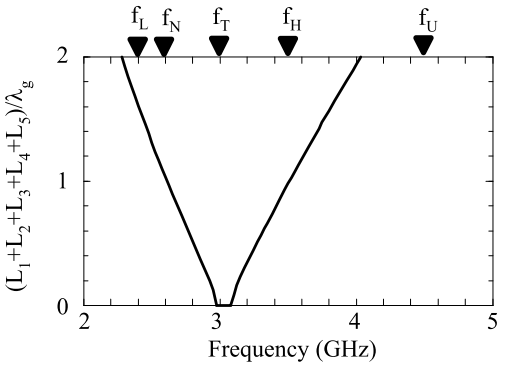

Fig. 3. Loop length $L_1 + L_2 + L_3 + L_4 + L_5$ normalized to guided wavelength λ_g, as a function of frequency. $\beta < 0$ at $f < f_T$, $\beta = 0$ at f_T, and $\beta > 0$ at $f > f_T$.

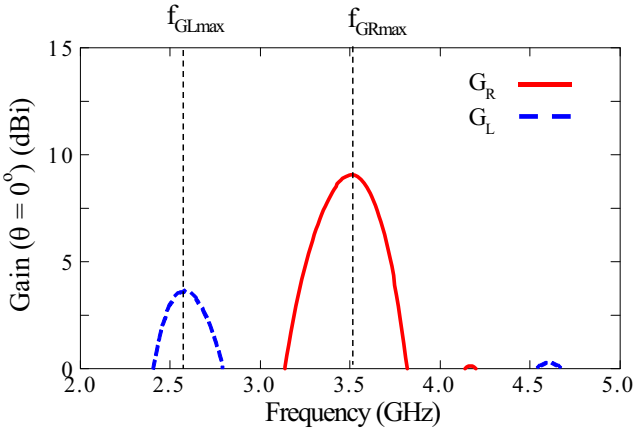

Fig. 4. Frequency response of the gain.

guided wavelength λ_g. In other words, the metaline acts as a leaky wave antenna. Generally, the radiation efficiency of the leaky wave antenna is not high due to absorption of the power input to the antenna by R_B. If R_B is removed, the input impedance (and hence Voltage Standing Wave Ratio (VSWR)) becomes unstable and CP radiation is not obtained by a reflected current from point T.

The current at frequency $f < f_T$ has a progressive phase distribution from point F to point T due to a negative phase constant ($\beta = -2\pi/\lambda_g < 0$). Hence, the current behaves as if it travels from point T to point F (clockwise). This results in LHCP radiation in the broadside direction at a frequency where the loop length is one guided wavelength ($1\lambda_g$). Conversely, the current at $f > f_T$ has a regressive phase distribution from point F to point T due to a positive phase constant ($\beta = 2\pi/\lambda_g > 0$). Hence, the current flows from point F to point T (counter clockwise), resulting in RHCP radiation in the broadside direction at a frequency satisfying a $1\lambda_g$-loop length. Thus, dual-band counter CP radiation in the broadside direction is obtained.

From Figure 3, it is expected that CP broadside radiation will be obtained around frequencies 2.60 GHz $\equiv f_N$ and 3.50 GHz $\equiv f_H$, because the loop length normalized to guided wavelength λ_g is one at f_N and f_H: $(L_1 + L_2 + ... + L_5)/\lambda_g = 1$. For the remainder of the paper, f_N and f_H are referred to as

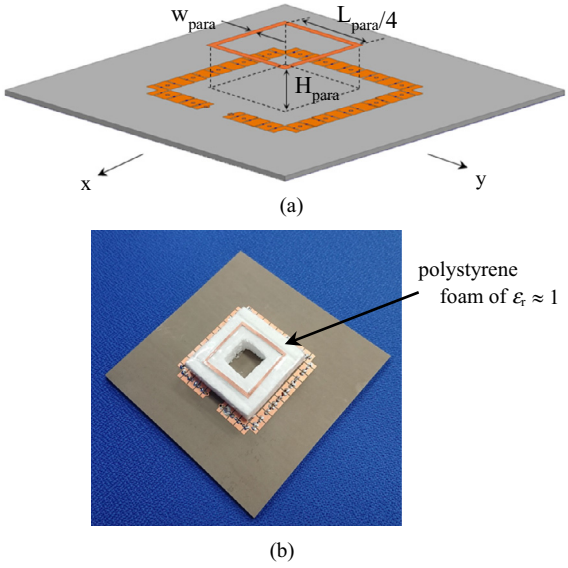

Fig. 5. Metaloop with a parasitic natural conducting loop. (a) Perspective view. (b) Fabricated metaloop.

the Nion frequency and Hion frequency, respectively. Figure 4 shows the gain as a function of frequency, where G_L denotes the gain for an LHCP wave, called the LHCP gain, and G_R denotes the gain for an RHCP wave, called the RHCP gain. It is found that G_L is dominant at frequencies below $f_T = 3$ GHz, because the current flows with a negative phase constant ($\beta < 0$). Conversely, G_R is dominant at frequencies above transition frequency f_T due to $\beta > 0$. Maximum gain G_L appears at a frequency near Nion frequency f_N and maximum gain G_R appears at a frequency near Hion frequency f_H. These frequencies are denoted as f_{GLmax} and f_{GRmax}, respectively. The difference in the maximum gains, G_{Lmax} at 2.58 GHz $\equiv f_{GLmax}$ (close to f_N) and G_{Rmax} at 3.51 GHz $\equiv f_{GRmax}$ (close to f_H), is approximately 5.5 dB.

4 Reduction in the gain difference

In this section, the difference in maximum gains G_{Lmax} and G_{Rmax} is reduced as much as possible. For this, the antenna system shown in Figure 5 is considered, where a parasitic natural conducting strip loop of width w_{para} and peripheral length L_{para} is located at height H_{para} above the metaloop. The parasitic loop is designed such that only the smaller gain, G_{Lmax} at f_{GLmax}, is increased, without reducing the larger gain, G_{Rmax} at f_{GRmax}.

The CP radiation from the metaloop excites the parasitic loop and generates a rotating/traveling current along the loop.

The parasitic loop acts as a director for the driven metaloop, like Yagi–Uda antenna. If the radiation from the parasitic loop at f_{GLmax} is constructively superimposed onto the radiation from the metaloop in the broadside direction, gain G_{Lmax} increases. For this to occur, parasitic loop length L_{para} is chosen to be one free-space wavelength ($1\lambda_0$) at f_{GLmax}: $L_{para} = 116.7$ mm. The remaining task is to optimize loop height H_{para}.

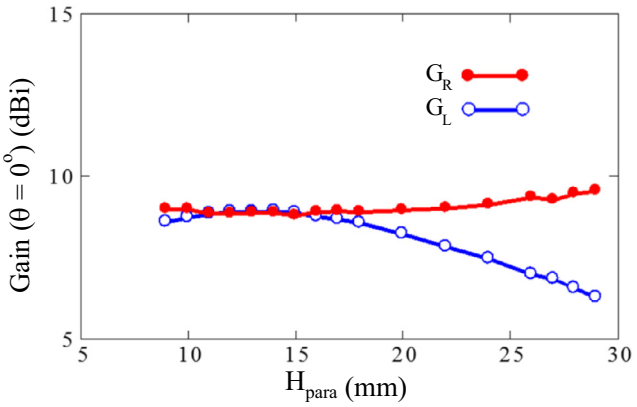

Fig. 6. G_L at $f = 2.58$ GHz and G_R at 3.51 GHz as a function of parasitic loop (paraloop) height H_{para}, where $w_{para} = 2$ mm and $L_{para} = 116.7$ mm ($\approx 1\lambda_0$ at 2.58 GHz) are used.

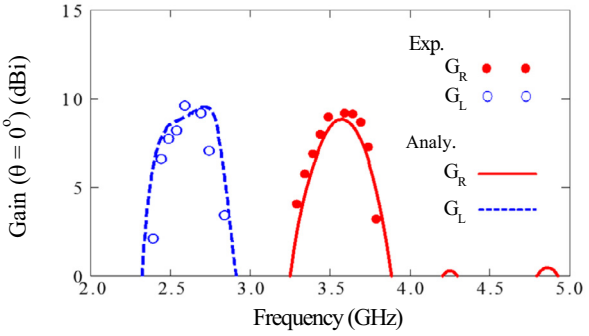

Fig. 7. Frequency response of the gain with a parasitic loop (paraloop), where $H_{para} = 11$ mm $= 0.09$ wavelength at $f_{GLmax} = 2.58$ GHz.

Figure 6 shows G_L at $f_{GLmax} = 2.58$ GHz and G_R at $f_{GRmax} = 3.51$ GHz in the broadside direction (z-direction) as a function of parasitic loop height H_{para}. It is found that there is an optimum antenna height for $G_{Lmax} \approx G_{Rmax}$.

Based on the result shown in Figure 6, the loop height is determined to be $H_{para} = 11$ mm, corresponding to 0.09 wavelength at $f_{GLmax} = 2.58$ GHz. Figure 7 shows the frequency response of the gain. The bandwidth (BW) for a 3-dB gain drop criterion for G_L, denoted as G_L-BW, is 13.5% and the BW for a 3-dB gain drop criterion for G_R, denoted as G_R-BW, is 14.6%. For confirmation of the analysis/simulation results, measured/experimental results are also presented (see fabricated antenna in Fig. 5b).

5 Radiation pattern and VSWR

Figure 8a shows the analysis/simulation results of the radiation patterns at the maximum-gain low frequency $f_{GLmax} = 2.58$ GHz (radiation efficiency of $\eta \approx 69\%$) and high frequency $f_{GRmax} = 3.51$ GHz ($\eta \approx 60\%$), together with experimental results, where E_L and E_R denote the LHCP wave component and the RHCP wave component, respectively. For comparison, the analysis/simulation results in the absence of a parasitic loop are also shown in Figure 8b. It is clearly seen that the radiation pattern at

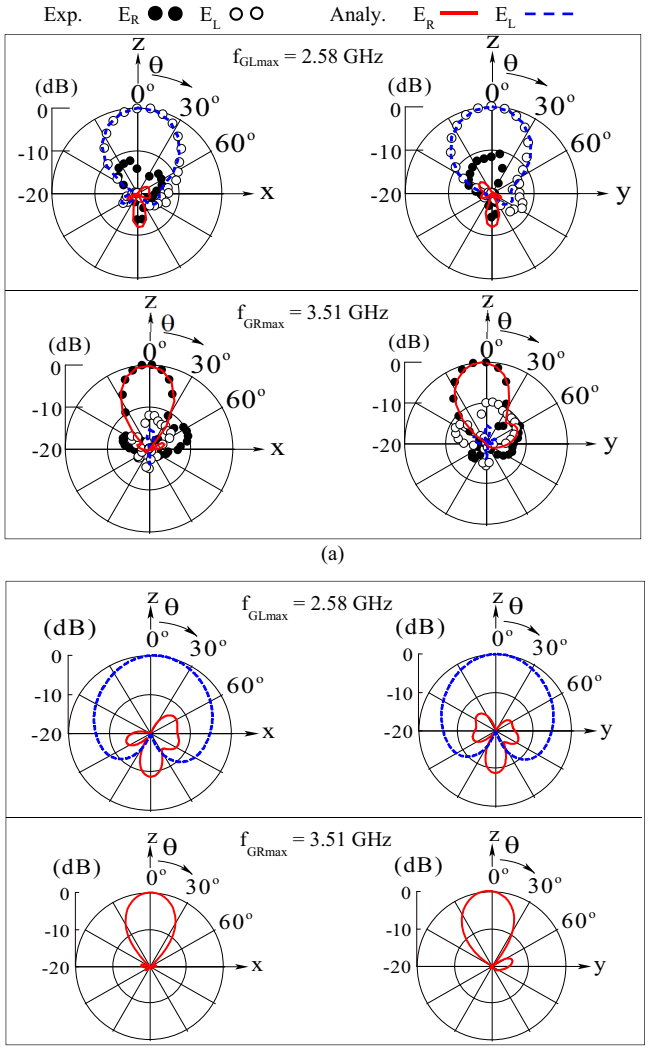

Fig. 8. Normalized radiation patterns at $f_{GLmax} = 2.58$ GHz and $f_{GRmax} = 3.51$ GHz. (a) In the presence of a parasitic loop. (b) In the absence of a parasitic loop.

low frequency f_{GLmax} is narrowed by virtue of the presence of the parasitic loop, while the radiation pattern at high frequency f_{GRmax} is less affected by the parasitic loop, as desired. Figure 9 shows the frequency response of the VSWR, which remains almost unchanged in the presence of the parasitic loop. Discrepancy between the analysis and experiment results is attributed to the fact that soldering the capacitive chips to the subwavelength segments is not uniform due to handwork.

Finally, the following comments are added. The metaloop antenna in this paper could be operated as a dual-band CP element with the same rotational sense (dual-band mono-CP radiation), although this is not our objective. Such dual-band mono-CP radiation is performed by introducing switching circuits to points F and T so that each point can be chosen to be either a feed point or a terminal point. (1) For dual-band mono-LHCP radiation, set points F and T to be the feed (fd) and terminal (trmnl) points, respectively, at low frequency $f_{low} < f_T$, which is

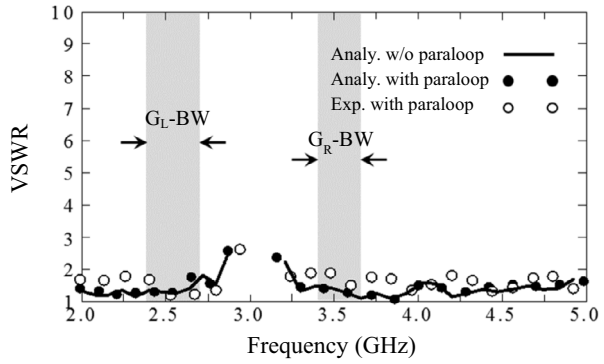

Fig. 9. Frequency response of the VSWRs in the presence and absence of a parasitic loop (paraloop). The 3-dB gain-drop bandwidths for G_{L} and G_{R} are denoted as G_{L}-BW and G_{R}-BW, respectively.

expressed as $[F:T]^{\mathrm{LHCP}}_{f_{\mathrm{low}}} = [\mathrm{fd}:\mathrm{trmnl}]$. And at a high frequency $f_{\mathrm{high}} > f_{\mathrm{T}}$, change the role of points F and T by using switching circuits: $[F:T]^{\mathrm{LHCP}}_{f_{\mathrm{high}}} = [\mathrm{trmnl}:\mathrm{fd}]$. (2) For dual-band mono-RHCP radiation, set $[F:T]^{\mathrm{RHCP}}_{f_{\mathrm{low}}} = [\mathrm{trmnl}:\mathrm{fd}]$ at f_{low} and $[F:T]^{\mathrm{RHCP}}_{f_{\mathrm{high}}} = [\mathrm{fd}:\mathrm{trmnl}]$ at f_{high} by using switch-circuits.

6 Conclusions

The dual-band counter CP wave radiated by a square metaloop antenna has a maximum gain of G_{Lmax} at frequency f_{GLmax} that is different from maximum gain G_{Rmax} at frequency f_{GRmax}, where $G_{\mathrm{Lmax}} < \mathrm{G}_{\mathrm{Rmax}}$. To reduce the difference in these gains, a square parasitic natural conducting loop of one free-space wavelength at f_{GLmax} is placed at height H_{para} above the metaloop. It is found that there is an antenna height where the parasitic loop increases gain G_{L}, while not remarkably affecting gain G_{R}. Thus, the gain difference can be reduced, i.e., $G_{\mathrm{Lmax}} \approx G_{\mathrm{Rmax}}$, with the VSWR remaining almost unchanged in the presence of the parasitic loop.

References

1. L.W. Rispin, D.C. Chang, Wire and loop F antennas, in: Y.T. Lo, S.W. Lee (Eds.), Antenna Handbook, Van Nostrand Reinhold Company Inc., NY 1988
2. H. Nakano, A numerical approach to line antennas printed on dielectric materials, Comput. Phys. Commun. **68**, 441 (1991)
3. H. Nakano, Y. Iitsuka, J. Yamauchi, Loop-based circularly polarized grid array antenna with edge excitation, IEEE Trans. Antennas Propag. **61**, 4045 (2013)
4. H. Nakano, K. Yoshida, J. Yamauchi, Radiation characteristics of a metaloop antenna, IEEE Antennas Wirel. Propag. Lett. **12**, 861 (2013)
5. C. Caloz, T. Itoh, Electromagnetic metamaterials (Wiley, NJ, 2006)
6. N. Engheta, R.W. Ziolkowski, Metamaterials (Wiley, NJ, 2006)
7. G.V. Eleftheriades, K.G. Balmain, Negative-refraction metamaterials: Fundamental principles and applications (Wiley, NY, 2005)
8. www.cybernet.co.jp/ansys/product/lineup/hfss
9. S.A. Rezaeieh, M.A. Antoniades, A.M. Abbosh, Gain enhancement of wideband metamaterial-loaded loop antenna with tightly coupled arc-shaped directors, IEEE Trans. Antennas Propag. **65**, 2090 (2017)
10. X. Zhao, Y. Lee, K.Y. Jung, J.H. Choi, Design of a metamaterial-inspired size-reduced wideband loop antenna with frequency scanning characteristic, IET Microw. Antennas Propag. **6**, 1227 (2012)
11. L.-M. Si, Q.-L. Zhang, W.-D. Hu, W.-H. Yu, Y.-M. Wu, X. Lv, W. Zhu, A uniplanar triple-band dipole antenna using complementary capacitively loaded loop, IEEE Antennas Wirel. Propag. Lett. **14**, 743 (2015)
12. Y. Zhang, K. Wei, Z. Zhang, Y. Li, Z. Feng, A compact dual-mode metamaterial-based loop antenna for pattern diversity, IEEE Antennas Wirel. Propag. Lett. **14**, 394 (2015)
13. B. Ghosh, S.K.M. Haque, D. Mitra, S. Ghosh, A loop loading technique for the miniaturization of non-planar and planar antennas, IEEE Trans. Antennas Propag. **58**, 2116 (2010)
14. S. Pandit, A. Mohan, P. Ray, A low-profile high-gain substrate-integrated waveguide-slot antenna with suppressed cross polarization using metamaterial, IEEE Antennas Wirel. Propag. Lett. **16**, 1614 (2017)
15. A.L. Borja, A. Belenguer, J. Cascon, J.R. Kelly, A reconfigurable passive UHF reader loop antenna for near-field and far-field RFID applications, IEEE Antennas Wirel. Propag. Lett. **11**, 580 (2012)
16. F.-Y. Meng, K. Zhang, J.-H. Fu, Q. Wu, J. Hua, Analogue of electromagnetically induced transparency in a magnetic metamaterial, IEEE Trans. Magn. **48**, 4390 (2012)
17. S.A. Rezaeieh, M.A. Antoniades, A.M. Abbosh, Bandwidth and directivity enhancement of loop antenna by nonperiodic distribution of mu-negative metamaterial unit cells, IEEE Trans. Antennas Propag. **64**, 3319 (2016)
18. K. Wei, Z. Zhang, Z. Feng, Design of a wideband horizontally polarized omnidirectional printed loop antenna, IEEE Antennas Wirel. Propag. Lett. **11**, 49 (2012)
19. Z.-G. Liu, Y.-X. Guo, Compact low-profile dual band metamaterial antenna for body centric communications, IEEE Antennas Wirel. Propag. Lett. **14**, 863 (2015)
20. X. Qing, C.K. Goh, Z.N. Chen, A broadband UHF near-field RFID antenna, IEEE Trans. Antennas Propag. **58**, 3829 (2010)

Cite this article as: Hisamatsu Nakano, Ittoku Yoshino, Tomoki Abe, Junji Yamauchi, Balanced gain for a square metaloop antenna, EPJ Appl. Metamat. **6**, 3 (2019)